Fluxonium: Single Cooper-Pair Circuit Free of Charge Offsets

Vladimir E. Manucharyan, *et al.*

Science **326**, 113 (2009);
DOI: 10.1126/science.1175552

Fluxonium: Single Cooper-Pair Circuit Free of Charge Offsets

Vladimir E. Manucharyan, Jens Koch, Leonid I. Glazman, Michel H. Devoret*

The promise of single Cooper-pair quantum circuits based on tunnel junctions for metrology and quantum information applications is severely limited by the influence of offset charges: random, slowly drifting microscopic charges inherent in many solid-state systems. By shunting a small junction with the Josephson kinetic inductance of a series array of large-capacitance tunnel junctions, thereby ensuring that all superconducting islands are connected to the circuit by at least one large junction, we have realized a new superconducting artificial atom that is totally insensitive to offset charges. Yet its energy levels manifest the anharmonic structure associated with single Cooper-pair effects, a useful component for solid-state quantum computation.

Electric charge can be manipulated at the level of a single charge quantum (*1*) in two types of superconducting circuits with different topologies. The minimal example of the first type of circuit is the Cooper-pair box, which consists of an isolated superconducting electrode (an "island") connected to a superconducting reservoir on one side by a small tunnel junction, and on the other side by a gate capacitance in series with a voltage source. The dynamics of the island is described by two variables: the integer number of Cooper pairs occupying the island and its conjugate, the 2π-cyclic superconducting phase difference between the island and the reservoir. The junction area must be sufficiently small that the electrostatic energy of the island due to an extra Cooper pair is larger than the Josephson energy of its coupling to the reservoir, thus confining fluctuations of the number of Cooper pairs below unity. Stated in electrical engineering language, one needs $Z_J > R_Q$, where the junction reactive impedance $Z_J = (L_J/C_J)^{1/2}$ is defined by the Josephson characteristic inductance L_J and capacitance C_J (*2*), and where the superconducting impedance quantum is given by $R_Q = \hbar/(2e)^2 \approx 1\ \mathrm{k}\Omega$, denoting Planck's constant $\hbar$ and the charge quantum e. The second type of circuit is based on a superconducting loop connecting the two electrodes of a small junction with an inductance that exceeds L_J. The circuit conjugate variables are now the magnetic flux generated by the persistent current in the loop and the displacement charge on the plates of the small junction capacitance. When $Z_J > R_Q$, the large loop inductance is submitted to quantum fluctuations of flux larger than the flux quantum $\Phi_0 = 2\pi\hbar/2e$; and therefore, according to the Heisenberg principle, the junction charge fluctuations are reduced below the value $2e$.

In practice, the realization of both circuit types faces fundamental difficulties. Islands are exposed to random electric fields due to fluctuating charged impurities, which are ubiquitous in most solid-state environments and whose compounded effect is described by a noisy offset charge. Although the fully developed charging effects were demonstrated for the Cooper-pair box (*3*, *4*), it soon became clear that the low-frequency offset charge noise was a major source of decoherence for charge qubits derived from this device (*4*–*7*). This state of affairs has prompted the development of alternative superconducting qubits based on large junctions with $Z_J << R_Q$, avoiding the single Cooper-pair regime and the related charge offset problem (*8*–*10*). On the other hand, implementing the island-free circuit, which is immune to charge offset noise, is another hard problem. This is because any finite-length wire with inductance L always comes with self-capacitance C, which reduces the total charging energy of the circuit and therefore steers it away from the charging regime, unless $(L/C)^{1/2} >> R_Q$. In fact, a purely electromagnetic inductance is incompatible with the single Cooper-pair effects, because $(L/C)^{1/2}$ is then bounded by the vacuum impedance $(\mu_0/\varepsilon_0)^{1/2} \approx 377\ \Omega < R_Q$, μ_0 and ε_0 being vacuum permeability and permittivity (*11*, *12*).

In this paper, we present experimental results from a novel single Cooper-pair circuit based on a superconducting loop, which solves both the inductance and the offset charge noise problems. The small junction of our circuit is shunted by a series array of carefully chosen larger-area tunnel junctions (Fig. 1, A to C). Here, all islands are connected to the rest of the circuit by at least one large junction, so that quasistatic offset charges on all islands are screened. The large capacitances of the array junctions prevent phase slips within the array, and at excitations whose frequencies are below the junction plasma frequency, the array effectively behaves as an inductive wire. By choosing a sufficiently large number of array junctions, it is possible to create an inductance exceeding that of the small junction. At low energies, the loop is effectively described by the loop flux $\hat{\Phi}$ and the small junction charge $\hat{Q}$, satisfying $[\hat{\Phi}, \hat{Q}] = i\hbar$.

To form a charge offset–free, inductively shunted junction, four conditions involving the effective inductance L_{JA} and capacitance C_{JA} of the N array junctions are required: (i) $NL_{JA} >> L_J$, (ii) $e^{-8R_Q/Z_{JA}} < \varepsilon << 1$, (iii) $Ne^{-8R_Q/Z_{JA}} << e^{-8R_Q/Z_J}$, and (iv) $N < (C_{JA}/C_g)^{1/2}$. In the relation (i), we simply estimate the total array inductance to be NL_{JA} and require that it exceed the small junction inductance, allowing it to support the large flux fluctuations of the loop. The relation (ii), where $Z_{JA} = (L_{JA}/C_{JA})^{1/2}$ is the array junction reactive impedance, dictates the minimum size of the array junctions necessary to reduce (*13*) the uncontrolled offset charge on the islands of the circuit below the desired value on the order of $2e \times \varepsilon$. The relation (iii) ensures that the inductive role of the array is not jeopardized by quantum phase slips (*14*). Specifically, the probability amplitude of a phase slip event within the array (l.h.s.) must be negligible compared to that in the small junction (r.h.s.). According to relation (iii), a fluxon tunnels in and out of the loop predominantly via the small junction, thus effectively erasing the discrete character of the array. Lastly, relation (iv) states that the inductance of the array is not shunted by the parasitic capacitances C_g of array islands to ground. It is obtained by estimating the array parasitic resonance frequency to be $(L_{JA}N \times C_gN)^{-1/2}$, and requiring that it be larger than the junction plasma frequency $(L_{JA}C_{JA})^{-1/2}$. It is relation (iv) which, with present junction technology, most severely limits the maximum number of junctions in the array and thus its maximum inductance.

We have implemented the above array proposal and constructed a new superconducting artificial atom which we have nicknamed fluxonium. It contains $N = 43$ Al/Al oxide/Al Josephson junctions (*15*), so that $Z_{JA} \cong 0.5\ R_Q$ and a small junction with $Z_J \cong 1.5\ R_Q$ (*16*). The above four conditions being realized, the fluxonium can be modeled (Fig. 1D) as a small junction shunted by an inductance L_A (*17*). The three characteristic energies of this model, namely $E_L = (\Phi_0/2\pi)^2/L_A$, $E_J = (\Phi_0/2\pi)^2/L_J$, and $E_C = e^2/(2\ C_J)$, have values corresponding to 0.52, 9.0, and 2.5 GHz, respectively. The additional L_RC_R resonator, capacitively connected to the small junction (Fig. 1D), reads out the atom in a manner analogous to the dispersive measurement of circuit quantum electrodynamics (cQED) qubits (*18*). It is implemented by a quarter-wave superconducting coupled microstrip resonator (Fig. 1A) with quality factor of 400, due to capacitive coupling to the two 50-Ω measurement ports. The resonator frequency $\omega_R = (L_RC_R)^{-1/2} \cong 2\pi \times 8.17$ GHz is pulled by the reactance of the fluxonium circuit and is monitored by a standard ultra–low-noise microwave reflection technique. The fluxonium reactance depends on its quantum state, an effect leading to a purely dispersive state measurement (*15*). An externally imposed, static magnetic flux Φ_{ext} threading the loop Φ_0 periodically modulates the spacings of energy levels of our artificial atom.

Departments of Physics and Applied Physics, Yale University, New Haven, CT 06520, USA.

*To whom correspondence should be addressed. E-mail: michel.devoret@yale.edu

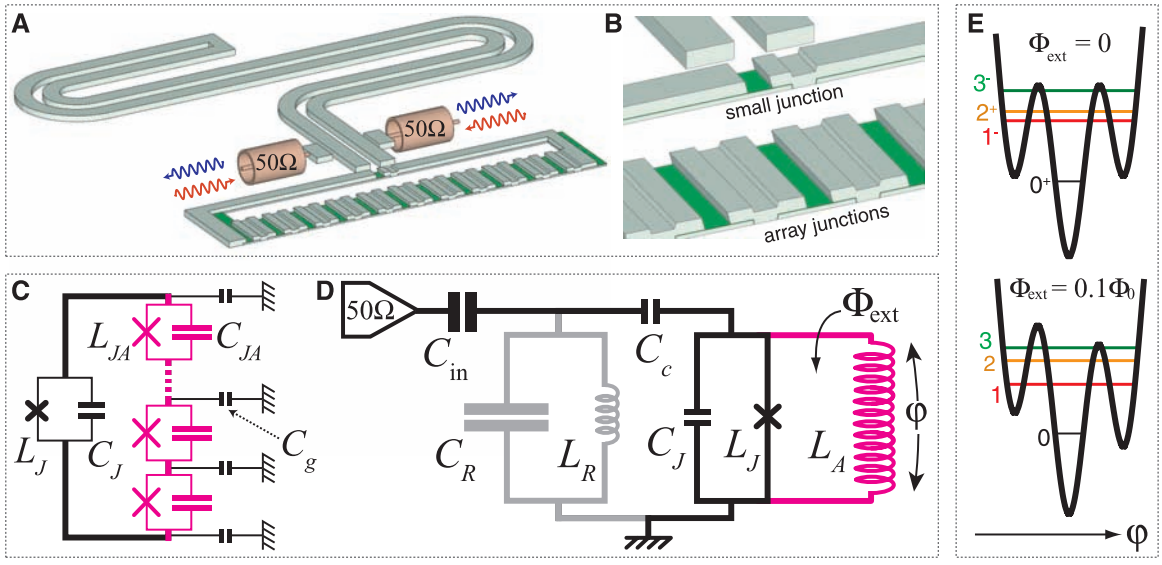

Fig. 1. (**A**) Sketch of a small Josephson junction shunted by an array of larger-area junctions. The two superconducting leads of the small junction are coupled capacitively to a quarter-wave microwave resonator, a parallel wire transmission line shorted on the opposite end. The resonator itself is probed capacitively and symmetrically via two 50-Ω microwave ports, resulting in a quality factor of 400. The whole device is made with single-step standard Al/Al oxide/Al double-angle evaporation through an e-beam lithography mask on a high-resistivity Si substrate. (**B**) Close-up view of the small junction region, showing top and bottom junction electrodes (gray) and their thin oxide layer (green). Array junctions are about one order of magnitude larger in area and are spaced as tightly as e-beam lithography resolution allows, minimizing microwave parasitics. (**C**) Electrical circuit representation of the loop formed by the small junction (black), with Josephson inductance L_J and capacitance C_J, shunted by the array of larger junctions (purple), with the corresponding inductance L_{JA} and capacitance C_{JA}. Islands formed between the array junctions have small capacitance to ground C_g. (**D**) Simplified circuit model of the fluxonium, consisting of three sections: (i) the circuit equivalent of a Cooper-pair box, where the small junction with capacitance C_J and nonlinear Josephson inductance L_J is capacitively (with capacitance C_c) coupled to the probe (solid black), so that $L_J/C_J)^{1/2} > \hbar/(2e)^2$; (ii) giant inductance $L_A >> L_J$ provided by the junction array (purple); (iii) a parallel combination of C_R and L_R so that $(L_R/C_R)^{1/2} \approx 50\ \Omega << \hbar/(2e)^2$, which is the circuit model for the distributed transmission line resonator (gray). (**E**) Potential seen by the reduced flux φ and energy spectrum of the circuit (D) for two values of external flux Φ_{ext}. At $\Phi_{ext} = 0$, energy levels possess well-defined parity as indicated with plus and minus signs next to the level numbers. In contrast with the RF-SQUID or flux qubit, there is on average only one level per local minimum.

Introducing the operators $\hat{N} = \hat{Q}/2e$ and $\hat{\varphi} = 2e\hat{\Phi}/\hbar$, describing the reduced charge on the junction capacitance and its conjugate reduced-flux operator (*19*), the Hamiltonian of the fluxonium coupled to its readout resonator can be written as

$$4E_C\hat{N}^2 + \frac{1}{2}E_L\hat{\varphi}^2 - E_J\cos(\hat{\varphi} - 2\pi\Phi_{ext}/\Phi_0) + g\hat{N}(\hat{a} + \hat{a}^\dagger) + \hbar\omega_R\hat{a}^\dagger\hat{a} \quad (1)$$

Here $\hat{a}$ is the photon annihilation operator for the resonator and g is the atom-resonator coupling constant. The second term and the range of definition of $\hat{\varphi}$ and $\hat{N}$, whose eigenvalues are here both on the entire real axis, distinguishes the form of Hamiltonian Eq. 1 from that of the Cooper-pair box in cQED experiments (*18*). There are three important points to note concerning this Hamiltonian (*20*): (i) It is invariant under the transformation $\hat{N} \rightarrow \hat{N} + N_{offset}$ (N_{offset} stands for offset charge value), hence the charge-free character of our device; (ii) it differs from that of the transmon (*13*), because offset charge influence is screened for all states, not just for the low-lying states; (iii) its second term, despite the fact that E_L is the smallest of the fluxonium energies, has a nonperturbative influence on the full energy spectrum of this artificial atom, which presents strongly anharmonic transitions (*21*) (Fig. 1E). Our experiment probes these transitions by microwave spectroscopy, from which we infer the size of charge fluctuations.

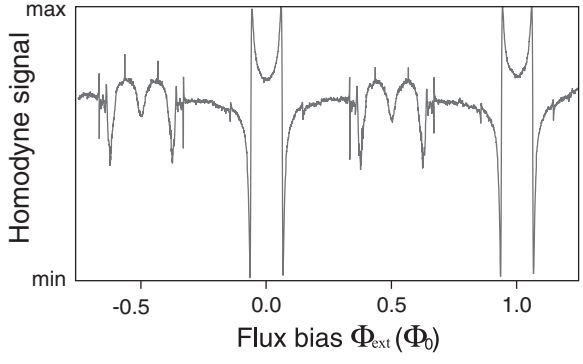

Fig. 2. Modulation of the reflected 8.18-GHz microwave signal with externally applied flux Φ_{ext}. The signal is clearly flux-periodic, indicating that the junction ring is closed and superconducting. The values of Φ_{ext} at which the signal undergoes full swings correspond to the anticrossings of the 0–1 transition frequency of the device with the resonator bare frequency, later inferred to be 8.1755 GHz. The measurement tone populates the resonator with less than 0.01 photon on average.

To characterize the fluxonium, we first measured the ground-state resonator pull as a function of Φ_{ext}. The results (Fig. 2) show the expected Φ_0 periodicity as well as the avoided crossings of the resonator frequency and the ground-to-excited–state transitions. This confirms that the entire 44-junction loop is superconducting and that the resonator-atom system is in the strong coupling regime of cavity QED (*22*).

Next, we performed a two-tone spectroscopy measurement (*23*) at a fixed flux $\Phi_{ext} = 0.05\ \Phi_0$, during which, in addition to the fixed frequency readout tone, we probed the transition frequencies of the atom through a second, variable-frequency spectroscopy tone. The resulting peaks (Fig. 3) correspond to the later-determined 0–1, 0–2, and 0–3 transitions from the atom ground state. The peaks are well-fitted by Lorentzians, and their power-dependent widths and heights are well explained by the Bloch equations of precessing spin 1/2 (*24*) (Fig. 3, insets). Extrapolating fitted line widths to zero spectroscopy power, we obtained lower bound estimates of their decoherence time at 350, 250, and 80 ns, respectively.

Our main result is the spectroscopic data collected as a function of both spectroscopy frequency and flux (Fig. 4A). Φ_{ext} variations span 20% of Φ_0 around $\Phi_{ext} = 0$ instead of the usual 1% or less around $\Phi_0/2$ in flux qubit experiments (*9*). In Fig. 4B, we compare the measured peak center frequencies with the prediction for the 0–1, 0–2, 0–3, and the two-photon 0–4 transitions obtained from numerical diagonalization of the Hamiltonian (Eq. 1). We are in effect fitting more than three flux-dependent

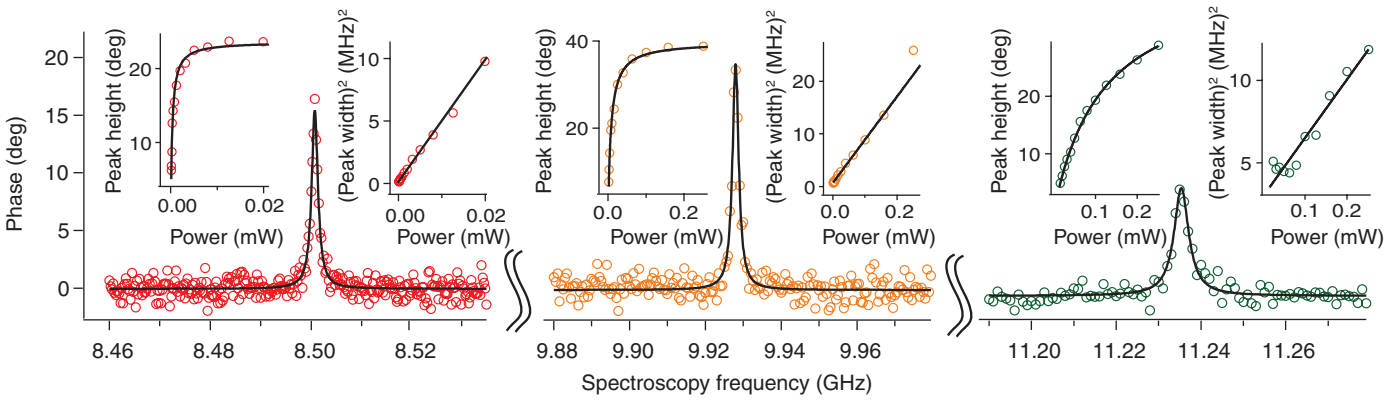

Fig. 3. Phase (colored circles) of reflected readout tone as a function of spectroscopy tone frequency taken at $\Phi_{ext} = 0.05\ \Phi_0$. Data for the first three resonances (further identified as transitions from the ground state to states 1, 2, and 3) are shown from left to right in red, orange, and green, respectively. Resonances are well fitted by Lorentzians (solid black lines) for a broad range of spectroscopy powers. Insets on the two sides of each resonance show the dependence of the resonant peak height (left) and width squared (right) on the spectroscopy tone power. Data in all insets follow the predictions (solid black lines) of Bloch equations describing relaxation dynamics for a spin 1/2 and indicate that all transitions involve one photon.

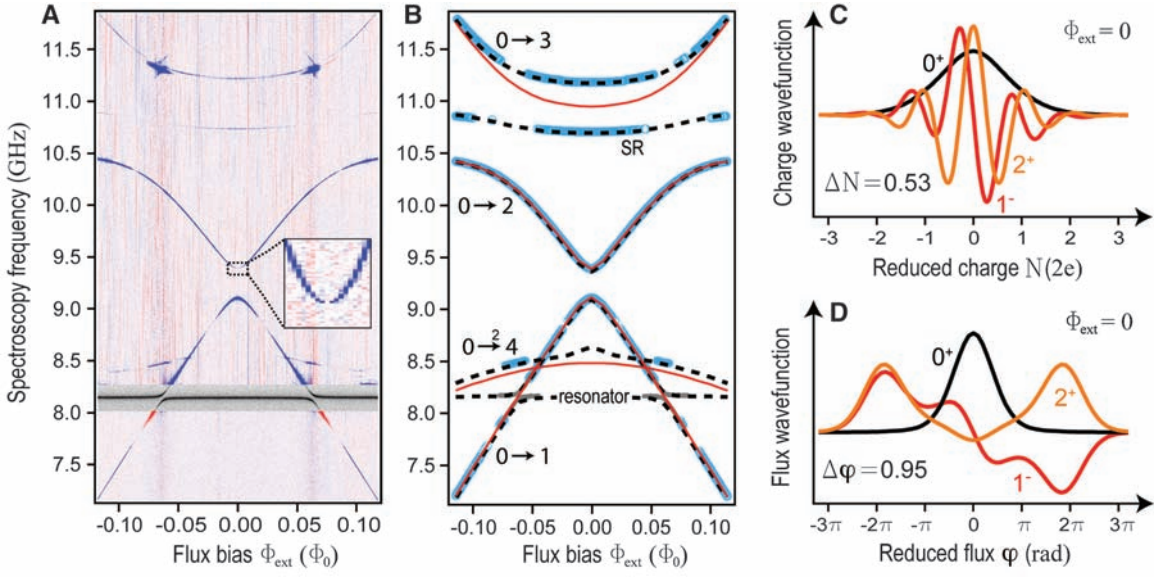

Fig. 4. (**A**) Phase of reflected readout tone as a function of the spectroscopy tone frequency and external flux. The color scale encodes the value of the phase, with zero corresponding to the mauve background, blue to positive values (peaks), and red to negative values (dips). The gray region shows the reflected phase of a single tone, swept close to the resonator bare frequency exhibiting a 50-MHz vacuum Rabi splitting of the resonator with the fluxonium transition 0–1. The inset in (A) zooms in on the central region of the 0–2 transition and confirms that it is indeed symmetry-forbidden at $\Phi_{ext} = 0$. (**B**) Measured peak frequencies (blue circles) fitted by the numerically computed spectrum of the Hamiltonian (Eq. 1) (solid red lines) and its modification (see supporting online text) to explain the additional transition labeled SR (dashed black lines). (**C**) Amplitude of fluxonium wave functions for levels 0 (black), 1 (red), and 2 (orange), computed in charge representation at zero flux bias, using circuit parameters extracted from the fits. (**D**) Same as in (C) but in flux representation. The flux representation wave functions demonstrate that the reduced flux is delocalized as compared to the size of the Josephson well, whereas charge wave functions confirm that the localization of charge on the junction is less than a single Cooper-pair charge. In this circuit, the junction charge is a continuous variable, in contrast to the Cooper-pair box, and flux swings of more than 2π are allowed.

functions (the flux-dependent transition frequencies) with only three a priori unknown energies E_C, E_L, and E_J, so the problem is severely overconstrained. The fit of the line (Fig. 4B) labeled SR (for array self-resonance) requires a minor extension of the model, taking into account parasitic capacitances across the array (*15*). Apart from introducing another resonator mode coupled to the atom, this extension by no means invalidates the inductive character of the array, at least as far as the 0–1 and 0–2 transition of the fluxonium are concerned. Even the perturbation of the 0–3 and 0–4 transition frequencies by this extra mode is less than 2%.

Based on the excellent agreement between theory and experiment, we inferred the wave functions of the first three energy levels and plotted their amplitudes both in charge (Fig. 4C) and flux (Fig. 4D) representations for $\Phi_{ext} = 0$. In the ground state, we find that the ratio of charge to flux fluctuations is $\Delta N/\Delta\varphi = 0.56$, about five times smaller than the fine structure constant allows for a conventional resonator. This confirms that the charge in our circuit is indeed localized at the single Cooper-pair level ($\Delta N = 0.53$, $\Delta\varphi = 0.95$). The wave functions in flux representation (Fig. 4D) can be interpreted as simple superpositions of states in which the reduced flux φ is localized in the wells of the Josephson cosine potential (fluxon states, hence the name fluxonium). The parity of fluxonium states, which forbids the 0–2 transition at zero external flux, manifests itself explicitly by a remarkable "hole" in the corresponding spectroscopic line (Fig. 4A, inset). The allowed transition between the second and third levels is particularly spectacular because it corresponds to motion of the total flux in the fluxonium loop by two whole flux quanta. This is to be contrasted with the 10% of flux quantum or less flux motion involved in transitions of the flux and phase qubits (*8*, *9*). Nevertheless, despite the large flux fluctuations of the system and the corresponding charge pinning, the circuit has complete immunity to offset charge variations: The data of Fig. 4A were taken piecemeal in 72 hours, and no jumps or drifts were observed during this period.

We have thus demonstrated that an array of Josephson junctions with appropriately chosen parameters can perform two functions simultaneously: short-circuit the offset charge variations of a small junction and protect the strong nonlinearity of its Josephson inductance from quantum fluctuations. The data show that the array possesses a microwave inductance 10^4 times larger than the geometric inductance of a wire of the same length (20 μm). The reactance of such an inductor is about 20 $R_Q \approx 20$ kΩ at 10 GHz, whereas its resistance is less than 1 Ω. The spectrum of the fluxonium qubit suggests that it is as anharmonic as the flux qubit but as insensitive to flux variations as the transmon qubit. Possible applications of this single Cooper-pair charging effect immune to charge noise include the observation of fully developed macroscopic quantum-coherent oscillations between fluxon states (*25*), the search for Λ or V transition configurations for the shelving of quantum information (*26*) in superconducting artificial atoms, topological protection of superconducting qubits (*27*), and, finally, the long-sought quantum metrology of electrical current via Bloch oscillations (*28*, *29*).

References and Notes

1. H. Grabert, M. H. Devoret, Eds., *Single Charge Tunneling: Coulomb Blockade Phenomena in Nanostructures* (Plenum, New York, 1992).
2. B. D. Josephson, *Rev. Mod. Phys.* **36**, 216 (1964).
3. V. Bouchiat, D. Vion, P. Joyez, D. Esteve, M. H. Devoret, *Phys. Scr.* **T76**, 165 (1998).
4. Y. Nakamura, Yu. A. Pashkin, J. S. Tsai, *Nature* **398**, 786 (1999).
5. D. Vion *et al.*, *Science* **296**, 886 (2002).
6. K. Bladh, T. Duty, D. Gunnarsson, P. Delsing, *N. J. Phys.* **7**, 180 (2005).
7. M. Metcalfe *et al.*, *Phys. Rev. B* **76**, 174516 (2007).
8. J. M. Martinis, S. Nam, J. Aumentado, C. Urbina, *Phys. Rev. Lett.* **89**, 117901 (2002).
9. I. Chiorescu, Y. Nakamura, C. J. P. M. Harmans, J. E. Mooij, *Science* **299**, 1869 (2003).
10. J. A. Schreier *et al.*, *Phys. Rev. B* **77**, 180502(R) (2008).
11. R. P. Feynman, R. B. Leighton, M. Sands, *The Feynman Lectures on Physics* (Addison-Wesley, Reading, MA, 1964), vol. 2, chap. 23.
12. The ratio $(\mu_0/\varepsilon_0)^{1/2}/R_Q = 16\pi\alpha$, where $\alpha \approx 1/137$ is the fine structure constant.
13. J. Koch *et al.*, *Phys. Rev. A* **76**, 042319 (2007).
14. K. A. Matveev, A. I. Larkin, L. I. Glazman, *Phys. Rev. Lett.* **89**, 096802 (2002).
15. Materials and methods are available as supporting material on *Science* Online.
16. Because of coupling of the fluxonium circuit to the readout resonator (Fig. 1D), C_J is renormalized to the value $C_J + C_c$, with corrections on the order of $C_c/C_R \cong 1\%$.
17. Here we acknowledge experiments (*30*, *31*) in which a small Josephson junction was dc-biased in series with a micrometer-scale disordered film resistance exceeding R_K (*30*) or with an array of small-junction superconducting quantum interference devices (SQUIDs) (*31*) with zero-bias resistance tuned by magnetic field to exceed R_K. Both experiments aimed at protecting the small junction from the shunting effect of a low-impedance environment, using highly dissipative biasing elements. Although the results of dc current-voltage measurements were consistent with single Cooper-pair effects, they were distorted by Joule heating and other out-of-equilibrium effects in these biasing elements. We avoid the problem of dissipation with an array employing the pure Josephson kinetic inductance.
18. A. Wallraff *et al.*, *Nature* **431**, 162 (2004).
19. M. Devoret, in *Quantum Fluctuations in Electrical Circuits*, S. Reynaud, E. Giacobiano, J. Zinn-Justin, Eds. (Elsevier Science, Amsterdam, 1997).
20. J. Koch, V. Manucharyan, L. Glazman, M. Devoret, available at http://arxiv.org/abs/0902.2980 (2009).
21. Although the circuit in Fig. 1D might appear identical to the radio frequency (RF)–SQUID circuit (*32*), there is a drastic difference between the two when charging, Josephson, and inductive energies are compared. In addition, RF-SQUID is addressed by coupling to its flux degree of freedom via mutual inductance, whereas the fluxonium is addressed by coupling to its charge degree of freedom via capacitance C_c.
22. J. Raimond, M. Brune, S. Haroche, *Rev. Mod. Phys.* **73**, 565 (2001).
23. D. I. Schuster *et al.*, *Phys. Rev. Lett.* **94**, 123602 (2005).
24. A. Abragam, *The Principles of Nuclear Magnetism* (Oxford Univ. Press, Oxford, 1961).
25. A. J. Leggett, *J. Phys. Condens. Matter* **14**, R415 (2002) and references therein.
26. W. Nagourney, J. Sandberg, H. Dehmelt, *Phys. Rev. Lett.* **56**, 2797 (1986).
27. A. Kitaev, available at http://arxiv.org/abs/condmat/0609441 (2006).
28. D. V. Averin, A. B. Zorin, K. K. Likharev, *Zh. Exp. Teor. Phys.* **88**, 692 (1985).
29. K. K. Likharev, A. B. Zorin, *J. Low Temp. Phys.* **59**, 347 (1985).
30. L. S. Kuzmin, D. B. Haviland, *Phys. Rev. Lett.* **67**, 2890 (1991).
31. M. Watanabe, D. B. Haviland, *Phys. Rev. Lett.* **86**, 5120 (2001).
32. J. R. Friedman, V. Patel, W. Chen, S. K. Tolpygo, J. E. Lukens, *Nature* **406**, 43 (2000).

33. We acknowledge discussions with M. Brink, E. Boaknin, M. Metcalfe, R. Vijay, D. Schuster, L. DiCarlo, L. Frunzio, R. Schoelkopf, and S. Girvin. This research was supported by NSF under grants DMR-0754613 and DMR-032-5580, the National Security Agency through ARO grant no. W911NF-05-01-0365, the Keck Foundation, and the Agence Nationale pour la Recherche under grant ANR07-CEXC-003. M.H.D. acknowledges partial support from the College de France.

Supporting Online Material

www.sciencemag.org/cgi/content/full/326/5949/113/DC1
Materials and Methods
SOM Text
Fig. S1
Table S1
References

29 April 2009; accepted 28 July 2009
10.1126/science.1175552

Preferential Growth of Single-Walled Carbon Nanotubes with Metallic Conductivity

Avetik R. Harutyunyan,[1]* Gugang Chen,[1] Tereza M. Paronyan,[2] Elena M. Pigos,[1] Oleg A. Kuznetsov,[1] Kapila Hewaparakrama,[2] Seung Min Kim,[3,4] Dmitri Zakharov,[4] Eric A. Stach,[3,4] Gamini U. Sumanasekera[2]

Single-walled carbon nanotubes can be classified as either metallic or semiconducting, depending on their conductivity, which is determined by their chirality. Existing synthesis methods cannot controllably grow nanotubes with a specific type of conductivity. By varying the noble gas ambient during thermal annealing of the catalyst, and in combination with oxidative and reductive species, we altered the fraction of tubes with metallic conductivity from one-third of the population to a maximum of 91%. In situ transmission electron microscopy studies reveal that this variation leads to differences in both morphology and coarsening behavior of the nanoparticles that we used to nucleate nanotubes. These catalyst rearrangements demonstrate that there are correlations between catalyst morphology and resulting nanotube electronic structure and indicate that chiral-selective growth may be possible.

Carbon nanotubes have yet to see ubiquitous application in electronic devices, despite their electronic properties (*1*). This is largely because the electronic properties are related to nanotube bonding configuration (known as its chirality). Though some methods exist to bias the population of one type of nanotube during synthesis, there is only a limited understanding of exactly what determines chirality during synthesis.

There have been important achievements in separating single-walled carbon nanotubes (SWNTs) according to their conductivity (*2*–*5*) and in enriching the distribution of nanotubes with a specific conductivity (*6*, *7*). Meanwhile, there have been a few reports regarding direct control over nanotube structure during growth (*8*–*10*). The fact that SWNTs with narrow chiral distributions have been successfully grown (*8*) indicates that there may be a specific mechanism that controls chirality. The concept of amplifying existing SWNT distributions by seeding growth from another nanotube with well-defined chirality has been proposed (*9*); however, evidence for the maintenance of chirality has not yet been reported (*10*). The preferential growth of nearly 90 (*11*) to 96% (*12*) of semiconducting SWNTs by plasma-enhanced chemical vapor deposition has been reported, but the mechanism that leads to this selectivity remains unclear.

In this work, we grew SWNTs from Fe nanocatalysts deposited onto a SiO_2/Si support

[1]Honda Research Institute USA, 1381 Kinnear Road, Columbus, OH 43212, USA. [2]Department of Physics and Astronomy, University of Louisville, Louisville, KY 40292, USA. [3]School of Materials Engineering, Purdue University, 701 Northwestern Avenue, West Lafayette, IN 47907, USA. [4]Birck Nanotechnology Center, Purdue University, 1205 West State Street, West Lafayette, IN 47907, USA.

*To whom correspondence should be addressed. E-mail: aharutyunyan@honda-ri.com